

Consistent picture of the octet-nodal gap and its evolution with doping in heavily overdoped $\text{Ba}_{1-x}\text{K}_x\text{Fe}_2\text{As}_2$

Shun-Li Yu, Zi-Jian Yao, and Jian-Xin Li

*National Laboratory of Solid State Microstructures and Department of Physics, Nanjing University, Nanjing 210093, China
Collaborative Innovation Center of Advanced Microstructures, Nanjing, China*

(Dated: February 29, 2024)

We investigate the pairing symmetry in heavily overdoped $\text{Ba}_{1-x}\text{K}_x\text{Fe}_2\text{As}_2$ based on the spin-fluctuation mechanism. The exotic octet nodes of the superconducting gap and the unusual evolution of the gap with doping observed by the recent experiments are well explained in a unified manner. We demonstrate that the scatterings of electrons on the Fermi patches is mainly responsible for the incommensurate spin fluctuations and consequently the Fermi-surface-dependent multi-gap structure, since the Fermi level is close to the flat band. In addition, we find that a d -wave pairing state will prevail over the s -wave pairing state around the Lifshitz transition point.

PACS numbers: 74.70.Xa, 74.20.Rp, 71.10.-w

Since the discovery of iron-based superconductors (FeSCs) in 2008 [1, 2], the mechanism underlying the superconductivity has been one of the most challenging problems. Despite great efforts, the pairing mechanism and the pairing symmetries are still under debate. The prevailing theoretical suggestion is that the electron pairing is mediated by the collinear antiferromagnetic spin-fluctuations and the superconducting (SC) gap changes sign between the hole and electron Fermi surfaces (FSs) (the so-called s_{\pm} state) in the underdoped and optimally doped regimes[3–7], though there are other proposals[8–10]. Recently, the over-hole-doped compounds $\text{Ba}_{1-x}\text{K}_x\text{Fe}_2\text{As}_2$ (BaK122) have attracted much attention, as they exhibit many anomalies deviating from the known FeSC trends. Thus, the understanding of the gap symmetries in these superconducting materials will provide more insights into the microscopic pairing mechanism in the FeSC.

KFe_2As_2 is the end member of the BaK122 series with $x = 1$. Unlike the optimally doped systems ($x = 0.4$), where the sizes of the electron and hole FSs are roughly equal, KFe_2As_2 has only the hole pockets centered at Γ point [$\mathbf{k} = (0, 0)$] but no electron pockets according to the angle-resolved photoemission spectroscopy (ARPES) measurements [11–13]. The absence of the electron pockets makes the s_{\pm} superconducting mechanism, which is mediated by the interband spin fluctuations between the hole and electron pockets, questionable in these heavily overdoped systems. A functional renormalization group study [14] suggests a d -wave superconducting state, while a random-phase-approximation (RPA) analysis [15] shows that the s_{\pm} -wave pairing is dominant but the d -wave is very close in energy. Experimentally, the thermal conductivity [16–18] and magnetic penetration-depth [19] measurements support the d -wave symmetry. However, the recent laser ARPES experiment observes a nodal s -wave state with an exotic FS-dependent multi-gap structure [11]: a nodeless gap with the largest magnitude on the inner FS, an unconventional gap with octet-

line nodes on the middle FS, and an almost-zero gap on the outer FS. These ARPES results are supported by thermodynamic experiments [20, 21]. Moreover, the more recent ARPES experiment [22] finds that the gap anisotropy on these FSs drastically changes with a small amount of electron doping. In particular, the gap on the middle FS becomes nodeless when the electron concentration is slightly increased, while the gap structure on the outer FS remains unchanged[22]. By assuming the dominant interaction at small momentum transfers, a particular kind of s -wave state was proposed [23], but it is hard to explain the evolution of gap structure with doping. Besides the multi-gap structures, the spin fluctuation also exhibits differences from that in optimally doped systems, where spin fluctuations are observed at the same q position $(\pi, 0)$ as the collinear SDW order wavevector at low energies[24]. By contrast, the spin fluctuation in overdoped BaK122 is incommensurate with the wavevector $(\pi \pm 0.32\pi, 0)$ as found by the recent inelastic neutron scattering (INS) experiments[25, 26].

These anomalous phenomena in heavily overdoped BaK122 raise the following issues: (i) How can we understand the complicated octet-node structures of the SC gap and its evolution with doping? (ii) What is the possible origin of the incommensurate spin fluctuations? (iii) Whether is the spin fluctuation mechanism applicable to these systems in which the electron pockets are absent. In this Letter, we provide a unified picture for the incommensurate spin fluctuations and the resulting unusual octet-node structures of the SC gap and its evolution with doping based on a weak-coupling calculation of the five-orbital Hubbard model. We find that the incommensurate spin fluctuation originates from the intra-orbital particle-hole excitations. Though the inter-orbital spin fluctuation does not show up in the physical spin susceptibility, it plays a role in the determination of the FS-dependent exotic SC gap structure. Besides the FS nesting, we find that the scatterings of electrons related to the Fermi patches play an essential role both in the

incommensurate spin fluctuation and SC gap structures, since the Fermi level is close to the flat band. In addition, although the s -wave pairing is the dominant pairing symmetry in a large doping range, a d -wave pairing state will be more favored around the Lifshitz transition point. Therefore, the long sought $s+id$ state is probably realized around this transition point.

The model Hamiltonian consists of two parts:

$$H = H_0 + H_{int}. \quad (1)$$

H_0 is the effective five-orbital tight-binding model in the unfolded Brillouin zone (BZ) developed by Graser *et al.*[27] to describe the energy band structure of the BaK122. It reads

$$H_0 = \sum_{\mathbf{k}, \sigma} \sum_{\alpha, \beta=1}^5 c_{\mathbf{k}\alpha\sigma}^\dagger H_{\alpha\beta}(\mathbf{k}) c_{\mathbf{k}\beta\sigma}, \quad (2)$$

where $c_{\mathbf{k}\alpha\sigma}^\dagger$ ($c_{\mathbf{k}\alpha\sigma}$) creates (annihilates) an electron with spin σ and momentum \mathbf{k} in the orbital α . The details of $H_{\alpha\beta}(\mathbf{k})$ can be found in Ref. 27. Fig. 1(a) shows the FS for the electron concentration $n = 5.5$ per Fe atom at $k_z = 0$. The relation between n and x is $n = 6 - 0.5x$, so $n = 5.5$ corresponds to KFe_2As_2 . Also shown in Fig. 1(a) is the intensity map of the bare single-particle spectral function $A(\mathbf{k}) = -\text{Im}[\text{Tr}\hat{G}(\mathbf{k}, \omega = 0)]/\pi$ with $\hat{G}(\mathbf{k}, \omega)$ the Green's function. We find that the orbital characters of the FS are consistent with the experimental results [11] and only a point-like FS appears around the X point. A characteristic of the electronic structure is that there is a flat band (saddle point) close to the Fermi level around X [Fig. 1(b)], which results in four Fermi patches (a region in the k space with a spectral intensity comparable to that on the FS) at $(0, \pm\pi)$ and $(\pm\pi, 0)$ as shown in Fig. 1(a). We note that recent ARPES experiment on heavily over-hole-doped BK122 do observe similar large spectral intensity around X [28]. The interactions between electrons in H_{int} are the standard multi-orbital on-site interactions (see Appendix A), which include the intra-orbital (inter-orbital) Coulomb interaction U (U'), the Hund's coupling J and the pairing hopping J' . In this paper, we choose $U = 0.6\text{eV}$, $U' = 0.3\text{eV}$ [27], and use the relations $J = J'$ and $U = U' + 2J$.

Based on the scenario that the pairing interaction in the FeSCs arises from the exchange of spin and charge fluctuations, we can calculate the effective electron-electron interaction using the RPA, which has been described in detail in the Appendix A. The singlet pairing interaction is given by

$$\hat{V}(q) = \frac{3}{2}\hat{U}^s\hat{\chi}^s(q)\hat{U}^s - \frac{1}{2}\hat{U}^c\hat{\chi}^c(q)\hat{U}^c + \frac{1}{2}(\hat{U}^s + \hat{U}^c), \quad (3)$$

where $\hat{\chi}^s$ ($\hat{\chi}^c$) is the spin (charge) susceptibility and \hat{U}^s (\hat{U}^c) is the interaction matrix for the spin (charge) fluctuation.

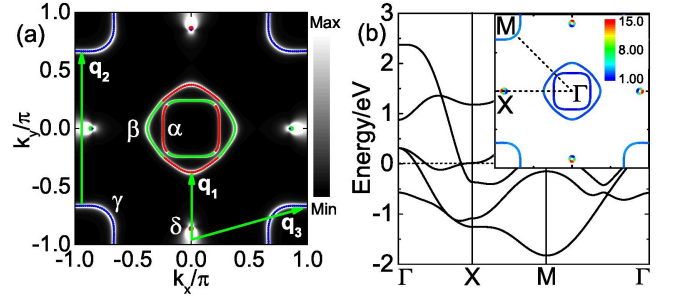


FIG. 1. (Color online) (a) FS in the unfolded BZ for KFe_2As_2 with $n = 5.5$ at $k_z = 0$. The dominant orbital weights along the FS are highlighted by colors (red: d_{xz} , green: d_{yz} , blue: d_{xy}). The grayscale image in the background shows the intensity of the spectral function $A(\mathbf{k})$. The lines with an arrow indicate the transferred wave vectors for the dominant particle-hole scatterings. The four sets of FSs are labeled by α , β , γ and δ , respectively. Here, the γ FS corresponds to the outer FS in the folded BZ observed by ARPES experiment according to its orbital characteristic. (b) Energy band structure. The dashed line indicates the Fermi level. The inset shows the density of state along the FS for $n = 5.55$.

We confine our considerations to the dominant scattering occurring in the vicinity of the FS. The scattering amplitude of a Cooper pair from the state $(\mathbf{k}, -\mathbf{k})$ on the FS i to the state $(\mathbf{k}', -\mathbf{k}')$ on the FS j is calculated from the projected interaction

$$\Gamma_{ij}(\mathbf{k}, \mathbf{k}') = \sum_{\mu\nu\eta\varphi} b_i^{\mu*}(-\mathbf{k}) b_i^{\nu*}(\mathbf{k}) \text{Re}[V_{\varphi\nu, \mu\eta}(\mathbf{k} - \mathbf{k}', \omega = 0)] \times b_j^\eta(\mathbf{k}') b_j^\varphi(-\mathbf{k}'), \quad (4)$$

where $b_i^\mu(\mathbf{k}) = \langle \mu, \mathbf{k} | i, \mathbf{k} \rangle$ projects the band basis $|i, \mathbf{k}\rangle$ to the orbital basis $|\mu, \mathbf{k}\rangle$. Here, i and μ are the band and orbital index respectively. We then solve the following eigenvalue problem:

$$-\sum_j \oint_{C_j} \frac{d\mathbf{k}'_{\parallel}}{4\pi^2 |\nabla E_j(\mathbf{k}')|} \Gamma_{ij}(\mathbf{k}, \mathbf{k}') g_j(\mathbf{k}') = \lambda g_i(\mathbf{k}), \quad (5)$$

where $E_j(\mathbf{k})$ is the energy of the tight-binding Hamiltonian (2) for the band j at the momentum \mathbf{k} and $g_i(\mathbf{k})$ is the normalized gap function along the FS i . The integral in Eq. (5) is evaluated along the FSs. The most favorable SC pairing symmetry corresponds to the gap function with the largest eigenvalue λ . One merit of this method is that it can adequately include the effect of DOS on the FS, which is very important in BaK122.

To resolve the eigenequation (5), we use 256 points along every hole-like FS and $16 \sim 128$ points along every electron-like FS depending on the size of the electron pocket. The temperature is set at $T = 0.005\text{eV}$, and the calculation of the susceptibility is done with uniform 128×128 meshes.

We will only discuss the spin fluctuations in the following because of the negligible role of charge fluctua-

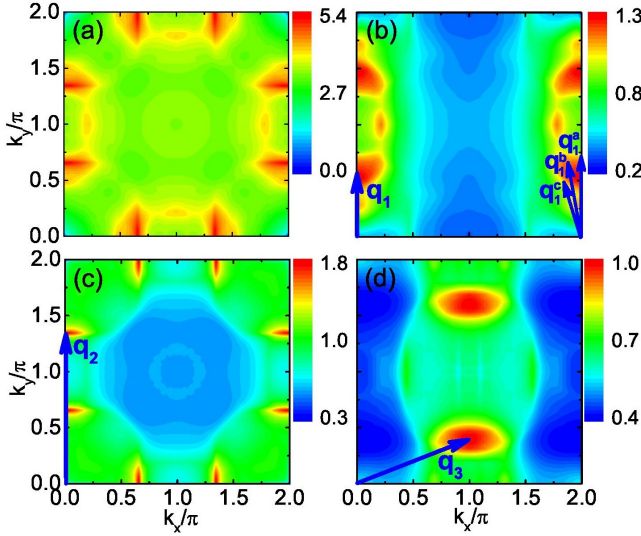


FIG. 2. (Color online) (a) Static physical spin susceptibility for $n = 5.5$. (b), (c) and (d) are the components which contribute mainly to the static spin susceptibility: (b) $\chi_{\mu\mu,\mu\mu}$ with $\mu = d_{xz}$; (c) $\chi_{\mu\mu,\mu\mu}$ with $\mu = d_{xy}$; (d) $\chi_{\mu\nu,\mu\nu}$ with $\mu = d_{xz}$ and $\nu = d_{xy}$. The vectors indicate the positions of the peaks in spin susceptibilities. q_1^a, q_1^b and q_1^c play basically the same role as q_1 due to the broad peak in χ .

tion. In Fig. 2, we present the spin susceptibility for $n = 5.5$. Fig. 2(a) is the static physical spin susceptibility $\tilde{\chi}^s(\mathbf{q}) = \sum_{\mu\nu} \chi_{\mu\mu,\nu\nu}^s(\mathbf{q}, \omega = 0)$, which corresponds to that measured by the neutron scattering experiments. It shows eight peaks located at the incommensurate wave vectors $(\pi \pm 0.34\pi, 0)$ and their symmetric points, which is consistent with the INS experiments on KFe_2As_2 [25, 26] and the previous theoretical result [15]. We find that $\tilde{\chi}^s$ is governed primarily by the intra-orbital spin fluctuations, and those within the d_{xz} , d_{yz} and d_{xy} orbitals contribute mainly to it, since the electronic states near the FS basically come from these three orbitals [Fig. 1(a)]. In Figs. 2(b) and (c), the intra-orbital spin fluctuations in the d_{xz} (that in the d_{yz} orbital is rotated by 90 degrees) and d_{xy} orbitals are presented. Usually, the spin fluctuations in the weak-coupling scheme is resulted from the particle-hole scatterings of electrons between the nesting FS. From the FS shown in Fig. 1(a), one can find that there is no nesting condition for the intra- d_{xz} -orbital spin fluctuation with the wavevector \mathbf{q}_1 [Fig. 2(b)]. Instead, we find that it is the scatterings of electrons between the β FS and the Fermi patches at $(0, \pm\pi)$ [Fig. 1(b)] contribute essentially to $\chi_{xzxx,xzxx}$. Whereas, the intra- d_{xy} -orbital spin fluctuation with \mathbf{q}_2 [Fig. 2(c)] is resulted from the nesting of the γ FS as shown in Fig. 1(a). The consequence of the Fermi-patch mechanism is that the peaks of χ in the d_{xz} orbital is much broader than those in the d_{xy} orbital. Another character is that in this doping level $\mathbf{q}_2 \approx 2\pi - \mathbf{q}_1$, so the peaks of the intra-orbital spin fluctuations in the d_{xz} and d_{xy} orbitals appear ba-

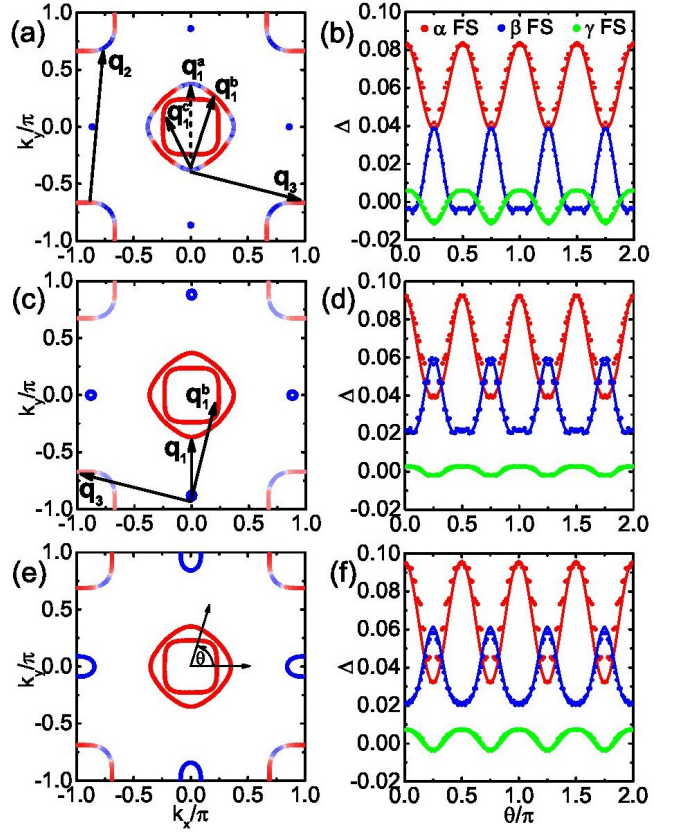


FIG. 3. (Color online) Dominant gap functions $g(\mathbf{k})$ and their sign structures along the FSs for different electron concentrations: (a) and (b) $n = 5.5$, (c) and (d) $n = 5.55$, (e) and (f) $n = 5.63$. In (a), (c) and (e), the signs of $g(\mathbf{k})$ are shown by the following colors: red (positive) and blue (negative). The arrows in (a) and (c) indicate the typical vectors related to the peaks of the spin fluctuations. (b), (d) and (f) show $g(\mathbf{k})$ as a function of the angular θ indicated in (e). The fittings of $g(\mathbf{k})$ are shown as the solid lines[see text].

sically at the same wave vectors. Besides, we find that the inter-orbital spin fluctuation $\chi_{\mu\nu,\mu\nu}$ where $\mu = d_{xz}$ (or d_{yz}) and $\nu = d_{xy}$ with the wavevector \mathbf{q}_3 also has a comparable magnitude with the intra-orbital spin fluctuations as shown in Fig. 2(d). It mainly comes from the scatterings of electrons between the γ FS and the Fermi patches near $(0, \pm\pi)$ as indicated by \mathbf{q}_3 in Fig. 1(a). Though not showing up in the physical spin susceptibility, this inter-orbital spin fluctuation is an important ingredient in determining the pairing symmetry.

The dominant pairing functions $g(\mathbf{k})$ and their sign structures obtained from Eq. (5) for three different electron concentrations are shown in Fig. 3. Figs. 3(a) and (b) show the results at $n = 5.5$ corresponding to the case of KFe_2As_2 . An obvious feature is that the gap function exhibits an unusual FS-dependent multi-gap structure. The gaps on the β and γ FSs reveal an eightfold sign reversal [Fig. 3(a)], whereas that on the α FS (the inner pocket) is nodeless. In addition, the magnitude of the

gap on the γ FS is much smaller than those on the α and β FSs [Fig. 3(b)]. With a slight increase of the electron concentration, we find that the gap anisotropy on these FSs drastically changes, as shown in Figs. 3(c-f) for $n = 5.55$ ($x = 0.9$) and $n = 5.63$ ($x = 0.74$). The octet node structure on the β FS disappears completely, and the gaps on both the β and α FSs are nodeless. While the gap on the γ FS still has the octet nodal structure. The obtained gap structure for KFe_2As_2 and its doping dependence are consistent with the recent laser ARPES results[11, 22]. Furthermore, the pairing functions on all three FSs can be well fitted in a unified manner with the function $g(\mathbf{k}) = \Delta(a_0 + a_1 \cos 4\theta + a_2 \cos 8\theta)$ [11], as shown by the solid lines in Fig. 3(b), (d) and (f) with the fitting parameters given in the Appendix B.

Within the spin-fluctuation mechanism, the pairing interaction in the spin-singlet channel is positive (repulsive)[see Eq. (3)]. Thus, the most favorable SC gap should satisfy the condition $g(\mathbf{k})g(\mathbf{k} + \mathbf{Q}) < 0$, where \mathbf{Q} is the typical wavevector at which the spin fluctuation has a peak. As the δ FS is very tiny for $n = 5.5$, it doesn't play a role in determining the gap signs. According to the general gap equation shown in the Appendix A, the scattering of a Cooper pair mediated by the intra-orbital spin fluctuation will happen between the FSs with the same orbital character. Due to the orbital weights of the α and β FSs shown in Fig. 1(a), three typical wavevectors \mathbf{q}_1^a , \mathbf{q}_1^b and \mathbf{q}_1^c , which correspond to the broad peak of the intra- d_{xz} -orbital spin fluctuation resulting from the scatterings of electrons in the Fermi patches, connect the FS pieces with the d_{xz} orbital character. Due to the symmetry constraint for the spin singlet pairing, the gap on the FS pieces connected by \mathbf{q}_1^a can not change sign. While, those on the FS pieces connected by \mathbf{q}_1^b and \mathbf{q}_1^c should change sign. Thus, it leads to the anomalous gap structures on the α and β FSs. This analysis is also applied to the sign change of $g(\mathbf{k})$ within the β FS connected by \mathbf{q}_2 which is the characteristic wavevector of the intra- d_{xy} -orbital spin fluctuation. While, the sign change between the β and γ FSs connected by \mathbf{q}_3 is required by the inter-orbital spin fluctuation as shown in Fig. 2(d).

With the increase of electron density, such as for $n = 5.55$ and $n = 5.63$, the Fermi level will be pushed towards the flat band. Consequently, the δ FS as well as the DOS on it will be enlarged. Though we do not find noticeable change in spin fluctuations correspondingly, the essential change is that now the δ FS plays an important role in determining the sign structure of $g(\mathbf{k})$. In Fig. 3(c), we plot the typical vectors by which the gaps on the connected FS change signs. The same situation happens for $n = 5.63$. In these cases, the gap function on the β FS is nodeless, while the sign structure of $g(\mathbf{k})$ on the γ FS remains the same as that for $n = 5.5$.

In fact, between $n = 5.55$ and $n = 5.63$, there is a Lifshitz transition from the small off- X -centered hole FS pocket lobes to that centered around the X ($0, \pi$) point,

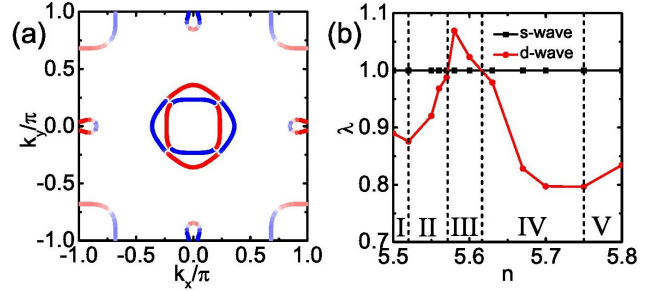


FIG. 4. (Color online) (a) The dominant gap function for $n = 5.6$. (b) The largest eigenvalues λ in the s -wave (normalized to 1) and d -wave channels as a function of the electron concentration n . The Roman numbers indicate the regions with different sign structures of the dominant gap function.

as can be seen from a comparison between Fig. 3(c) and Fig. 3(e). This Lifshitz transition has also been confirmed by the ARPES experiment [28]. Interestingly, we find that a d -wave pairing state will prevail over the s -wave state around the transition point, as seen from Fig. 4(a) where the most favorable gap structure for $n = 5.6$ is shown. The reason is that the DOS on the δ FS near X point is divergent at the transition point, which makes the gap function of the δ FS changes its signs between $(0, \pi)$ and $(\pi, 0)$ points according to Eq. (5). Besides this requirement, in fact, the typical vectors by which the gaps on the connected FS change signs are the same as those at $n = 5.5$ shown in Fig. 3(c). The only difference is that the sign structure is antisymmetric along the \mathbf{k}_x and \mathbf{k}_y directions in this case, while it is symmetric at $n = 5.5$ and $n = 5.63$. Without the addition requirement, in the latter case the nodeless gap on both the α and β FSs is favored energetically.

A detailed evolution of the gap symmetry with doping is presented in Fig. 4(b), where the two leading eigenvalues of the gap function Eq. (5) is shown (the optimal doping is $n = 5.8$). We can identify five regions according to the symmetry and sign structure of the gap. In region (I), the gap is s -wave with octet nodes on both β and γ FSs [Fig. 3(a)]. In regions (II) and (IV), the gap is s -wave with octet nodes only on the γ FS [Fig. 3(c) and (e)]. In region (III), the gap is d -wave [Fig. 4(a)]; In region (V), the gap is nodeless s_{\pm} -wave and the peaks of spin fluctuations are at $(0, \pm\pi)$ and $(\pm\pi, 0)$ [27]. Considering the near degeneracy of the s and d wave, we propose that the long sought $s + id$ pairing state in FeSC [29–35] would be probably realized in the heavily overdoped BaK122 around the Lifshitz transition point.

In summary, the pairing symmetry in the heavily overdoped $\text{Ba}_{1-x}\text{K}_x\text{Fe}_2\text{As}_2$ is studied based on the spin-fluctuation mechanism. The exotic octet nodes of the superconducting gap and the unusual evolution of the gap with doping observed by the recent experiments are explained in a unified manner. The scattering of elec-

trons related to the Fermi patches is demonstrated to be mainly responsible for the incommensurate spin fluctuations and consequently the gap structure. This Fermi-patch scenario provides a new viewpoint based on the large density of states resulting from the flat band, instead of the usual Fermi-surface-nesting picture where the Fermi surface topology is essential.

This work was supported by the National Natural Science Foundation of China (91021001, 11190023 and 11204125) and the Ministry of Science and Technology of China (973 Project Grants No.2011CB922101 and No.2011CB605902).

APPENDIX A: RANDOM PHASE APPROXIMATION (RPA) FOR MULTIORBITAL SYSTEM

The multiorbital Hubbard model we considered is given by

$$H = H_0 + H_{int}. \quad (6)$$

H_0 is the effective Hamiltonian without interactions, and H_{int} can be written as

$$\begin{aligned} H_{int} = & U \sum_{i\mu} n_{i\mu\uparrow} n_{i\mu\downarrow} + U' \sum_{i,\mu<\nu} \sum_{\sigma\sigma'} n_{i\mu\sigma} n_{i\nu\sigma'} \\ & + J \sum_{i,\mu<\nu} \sum_{\sigma\sigma'} c_{i\mu\sigma}^\dagger c_{i\nu\sigma'}^\dagger c_{i\mu\sigma'} c_{i\nu\sigma} \\ & + J' \sum_{i,\mu<\nu} c_{i\mu\uparrow}^\dagger c_{i\mu\downarrow}^\dagger c_{i\nu\downarrow} c_{i\nu\uparrow}, \end{aligned} \quad (7)$$

where $n_{i\mu\sigma} = c_{i\mu\sigma}^\dagger c_{i\mu\sigma}$ is the density operator at site i of spin σ in orbital μ . U (U') is the intra-orbital (inter-orbital) Coulomb interaction, J and J' are the Hund's coupling and the pairing hopping respectively.

The effective pairing interaction mediated by spin and charge fluctuations in the spin-singlet pairing channel is given by

$$\hat{V}(q) = \frac{3}{2} \hat{U}^s \hat{\chi}^s(q) \hat{U}^s - \frac{1}{2} \hat{U}^c \hat{\chi}^c(q) \hat{U}^c + \frac{1}{2} (\hat{U}^s + \hat{U}^c), \quad (8)$$

where $\hat{\chi}^s$ ($\hat{\chi}^c$) is the spin (charge) susceptibility and \hat{U}^s (\hat{U}^c) is the interaction matrix for the spin (charge) fluctuation. In RPA, the spin susceptibility $\hat{\chi}^s$ and charge susceptibility $\hat{\chi}^c$ are expressed as

$$\hat{\chi}^s(q) = [1 - \hat{\chi}^0(q) \hat{U}^s]^{-1} \hat{\chi}^0(q) \quad (9)$$

and

$$\hat{\chi}^c(q) = [1 - \hat{\chi}^0(q) \hat{U}^c]^{-1} \hat{\chi}^0(q) \quad (10)$$

respectively. The non-interacting susceptibility $\hat{\chi}^0$ is given by

$$\hat{\chi}_{\mu\nu,\eta\varphi}^0(q) = -\frac{T}{N} \sum_k G_{\eta\mu}(k+q) G_{\nu\varphi}(k) \quad (11)$$

with the number of lattice sites N and temperature T . The Green's function is given by

$$\hat{G}(k) = [i\omega_n - \hat{H}_0(\mathbf{k}) + \mu]^{-1}. \quad (12)$$

For an m -orbital system, the Green's function \hat{G} is a $m \times m$ matrix, while the susceptibilities $\hat{\chi}^0$, $\hat{\chi}^s$, $\hat{\chi}^c$ and the interactions $\hat{V}(q)$, \hat{U}^s , \hat{U}^c are $m^2 \times m^2$ matrices. In the above, $k \equiv (\mathbf{k}, i\omega_n)$ with $\omega_n = \pi T(2n+1)$. The interaction matrices \hat{U}^s and \hat{U}^c are given by:

$$U_{\mu\nu,\eta\varphi}^s = \begin{cases} U, & \mu = \nu = \eta = \varphi, \\ J, & \mu = \nu \neq \eta = \varphi, \\ U', & \mu = \eta \neq \nu = \varphi, \\ J', & \mu = \varphi \neq \nu = \eta, \\ 0, & \text{otherwise,} \end{cases} \quad (13)$$

$$U_{\mu\nu,\eta\varphi}^c = \begin{cases} U, & \mu = \nu = \eta = \varphi, \\ 2U' - J, & \mu = \nu \neq \eta = \varphi, \\ -U' + 2J, & \mu = \eta \neq \nu = \varphi, \\ J', & \mu = \varphi \neq \nu = \eta, \\ 0, & \text{otherwise.} \end{cases} \quad (14)$$

In the orbital representation, the superconducting gap equation (the ‘‘Eliashberg’’ equation) is given by

$$\begin{aligned} \lambda \Delta_{mn}(k) = & -\frac{T}{N} \sum_q \sum_{\alpha\beta} \sum_{\mu\nu} V_{\alpha m, n\beta}^{s,t}(q) G_{\alpha\mu}(k-q) \\ & \times G_{\beta\nu}(q-k) \Delta_{\mu\nu}(k-q). \end{aligned} \quad (15)$$

The most favorable superconducting pairing function is the eigenvector $\Delta_{mn}(k)$ with the largest eigenvalue λ .

Considering that the dominant scatterings of electrons occur in the vicinity of the Fermi surface (FS), we can reduce the effective interaction (8) and the ‘‘Eliashberg’’ equation (15) to the FS. The scattering amplitude of a Cooper pair between two points at the FS $[(\mathbf{k}, -\mathbf{k}) \rightarrow (\mathbf{k}', -\mathbf{k}')] is given by$

$$\begin{aligned} \Gamma_{ij}(\mathbf{k}, \mathbf{k}') = & \sum_{\mu\nu\eta\varphi} b_i^{\mu*}(-\mathbf{k}) b_i^{\nu*}(\mathbf{k}) \text{Re}[V_{\varphi\nu,\mu\eta}(\mathbf{k} - \mathbf{k}', \omega=0)] \\ & \times b_j^\eta(\mathbf{k}') b_j^\varphi(-\mathbf{k}'), \end{aligned} \quad (16)$$

where $b_i^\mu(\mathbf{k}) = \langle \mu, \mathbf{k} | i, \mathbf{k} \rangle$ projects the band basis $|i, \mathbf{k}\rangle$ to the orbital basis $|\mu, \mathbf{k}\rangle$. Here, i and μ are the band and orbital index respectively. In the calculations, we use the retarded Green's function and susceptibility by performing a Wick rotation $i\omega_n \rightarrow \omega + i\eta$. Then, the ‘‘Eliashberg’’ equation (15) is reduced to

$$-\sum_j \oint_{C_j} \frac{d\mathbf{k}'_{\parallel}}{4\pi^2 |\nabla E_j(\mathbf{k}')|} \Gamma_{ij}(\mathbf{k}, \mathbf{k}') g_j(\mathbf{k}') = \lambda g_i(\mathbf{k}), \quad (17)$$

where $E_j(\mathbf{k})$ is the energy of the band j at the momentum \mathbf{k} and $g_i(\mathbf{k})$ is the normalized gap function along the FS i . The integral in Eq. (17) is evaluated along the FSs.

APPENDIX B: FITTING PARAMETERS OF PAIRING FUNCTIONS

The pairing functions on different FS from our calculations can be fitted by a unified function: $g_i(k) = \Delta_i(a_{i0} + a_{i1} \cos 4\theta + a_{i2} \cos 8\theta)$, where i ($= \alpha, \beta$ or γ) represents one of the hole FSs. The fitting parameters for three typical electron concentrations $n = 5.5, 5.55$ and 5.63 in Fig. 3 of the main text are list in Table I. Though the $\cos 4\theta$ term dominates the octet-node structure, the $\cos 8\theta$ term also plays an important role, especially for the β Fermi surface at $n = 5.5$.

TABLE I. Parameters in fitting the pairing functions.

n	FS	a_0	a_1	a_2
5.5	α	0.061	0.023	0
5.5	β	0.01	-0.021	0.008
5.5	γ	0.0015	0.009	-0.001
5.55	α	0.063	0.027	0.003
5.55	β	0.034	-0.0185	0.007
5.55	γ	0.0005	0.0025	0
5.63	α	0.064	0.032	0
5.63	β	0.036	-0.02	0.005
5.63	γ	0.0022	0.0057	-0.0005

- [1] Y. Kamihara, T. Watanabe, M. Hirano, and H. Hosono, *J. Am. Chem. Soc.* **130**, 3296 (2008).
- [2] X. H. Chen, T. Wu, G. Wu, R. H. Liu, H. Chen, and D. F. Fang, *Nature(London)* **453**, 761 (2008).
- [3] I. I. Mazin, D. J. Singh, M. D. Johannes, and M. H. Du, *Phys. Rev. Lett.* **101**, 057003 (2008).
- [4] K. Kuroki, S. Onari, R. Arita, H. Usui, Y. Tanaka, H. Kontani, and H. Aoki, *Phys. Rev. Lett.* **101**, 087004 (2008).
- [5] Z. J. Yao, J. X. Li, and Z. D. Wang, *New J. Phys.* **11**, 025009 (2009).
- [6] F. Wang, H. Zhai, Y. Ran, A. Vishwanath, and D.-H. Lee, *Phys. Rev. Lett.* **102**, 047005 (2009).
- [7] S. Graser, T. A. Maier, P. J. Hirschfeld, and D. J. Scalapino, *New J. Phys.* **11**, 025016 (2009).
- [8] H. Kontani and S. Onari, *Phys. Rev. Lett.* **104**, 157001 (2010).
- [9] K. J. Seo, B. A. Bernevig, and J. P. Hu, *Phys. Rev. Lett.* **101**, 206404 (2008).
- [10] Q. M. Si and E. Abrahams, *Phys. Rev. Lett.* **101**, 076401 (2008).
- [11] K. Okazaki, Y. Ota, Y. Kotani, W. Malaeb, Y. Ishida, T. Shimojima, T. Kiss, S. Watanabe, C.-T. Chen, K. Kihou, C. H. Lee, A. Iyo, H. Eisaki, T. Saito, H. Fukazawa, Y. Kohori, K. Hashimoto, T. Shibauchi, Y. Matsuda, H. Ikeda, H. Miyahara, R. Arita, A. Chainani, S. Shin, *Science* **337**, 1314 (2012).
- [12] T. Yoshida, I. Nishi, A. Fujimori, M. Yi, R. G. Moore, D.-H. Lu, Z.-X. Shen, K. Kihou, P. M. Shirage, H. Kito, C.H. Lee, A. Iyo, H. Eisaki, H. Harima, *J. Phys. Chem. Solids* **72**, 465 (2011).
- [13] T. Sato, K. Nakayama, Y. Sekiba, P. Richard, Y.-M. Xu, S. Souma, T. Takahashi, G. F. Chen, J. L. Luo, N. L. Wang, and H. Ding, *Phys. Rev. Lett.* **103**, 047002 (2009).
- [14] R. Thomale, C. Platt, W. Hanke, J. Hu, and B. Andrei Bernevig, *Phys. Rev. Lett.* **107**, 117001 (2011).
- [15] K. Suzuki, H. Usui, and K. Kuroki, *Phys. Rev. B* **84**, 144514 (2011).
- [16] J. K. Dong, S. Y. Zhou, T. Y. Guan, H. Zhang, Y. F. Dai, X. Qiu, X. F. Wang, Y. He, X. H. Chen, and S. Y. Li, *Phys. Rev. Lett.* **104**, 087005 (2010).
- [17] J.-Ph. Reid, M. A. Tanatar, A. Juneau-Fecteau, R. T. Gordon, S. René de Cotret, N. Doiron-Leyraud, T. Saito, H. Fukazawa, Y. Kohori, K. Kihou, C. H. Lee, A. Iyo, H. Eisaki, R. Prozorov, and L. Taillefer, *Phys. Rev. Lett.* **109**, 087001 (2012).
- [18] A. F. Wang, S. Y. Zhou, X. G. Luo, X. C. Hong, Y. J. Yan, J. J. Ying, P. Cheng, G. J. Ye, Z. J. Xiang, S. Y. Li, and X. H. Chen, *Phys. Rev. B* **89**, 064510 (2014).
- [19] K. Hashimoto, A. Serafin, S. Tonegawa, R. Katsumata, R. Okazaki, T. Saito, H. Fukazawa, Y. Kohori, K. Kihou, C. H. Lee, A. Iyo, H. Eisaki, H. Ikeda, Y. Matsuda, A. Carrington, and T. Shibauchi, *Phys. Rev. B* **82**, 014526 (2010).
- [20] F. Hardy, R. Eder, M. Jackson, D. Aoki, C. Paulsen, T. Wolf, P. Burger, A. Böhrer, P. Schweiss, P. Adelman, R. A. Fisher, C. Meingast, *J. Phys. Soc. Jpn.* **83**, 014711 (2014).
- [21] D. Watanabe, T. Yamashita, Y. Kawamoto, S. Kurata, Y. Mizukami, T. Ohta, S. Kasahara, M. Yamashita, T. Saito, H. Fukazawa, Y. Kohori, S. Ishida, K. Kihou, C. H. Lee, A. Iyo, H. Eisaki, A. B. Vorontsov, T. Shibauchi, and Y. Matsuda, *Phys. Rev. B* **89**, 115112 (2014).
- [22] Y. Ota, K. Okazaki, Y. Kotani, T. Shimojima, W. Malaeb, S. Watanabe, C.-T. Chen, K. Kihou, C. H. Lee, A. Iyo, H. Eisaki, T. Saito, H. Fukazawa, Y. Kohori, and S. Shin, *Phys. Rev. B* **89**, 081103 (2014).
- [23] S. Maiti, M. M. Korshunov, and A. V. Chubukov, *Phys. Rev. B* **85**, 014511 (2012).
- [24] For a review, see P. Dai, J. P. Hu, and E. Dagotto, *Nat. Phys.* **8**, 709 (2012).
- [25] C. H. Lee, K. Kihou, H. Kawano-Furukawa, T. Saito, A. Iyo, H. Eisaki, H. Fukazawa, Y. Kohori, K. Suzuki, H. Usui, K. Kuroki, and K. Yamada, *Phys. Rev. Lett.* **106**, 067003 (2011).
- [26] J.-P. Castellán, S. Rosenkranz, E. A. Goremychkin, D. Y. Chung, I. S. Todorov, M. G. Kanatzidis, I. Eremin, J. Knolle, A. V. Chubukov, S. Maiti, M. R. Norman, F. Weber, H. Claus, T. Guidi, R. I. Bewley, and R. Osborn, *Phys. Rev. Lett.* **107**, 177003 (2011).
- [27] S. Graser, A. F. Kemper, T. A. Maier, H.-P. Cheng, P. J. Hirschfeld, and D. J. Scalapino, *Phys. Rev. B* **81**, 214503 (2010).
- [28] N. Xu, P. Richard, X. Shi, A. van Rooykeghem, T. Qian, E. Razzoli, E. Rienks, G.-F. Chen, E. Ieki, K. Nakayama, T. Sato, T. Takahashi, M. Shi, and H. Ding, *Phys. Rev. B* **88**, 220508 (2013).
- [29] W.-C. Lee, S.-C. Zhang, and C. Wu, *Phys. Rev. Lett.* **102**, 217002 (2009).
- [30] V. Stanev and Z. Tešanović, *Phys. Rev. B* **81**, 134522 (2010).
- [31] C. Platt, R. Thomale, C. Honerkamp, S.-C. Zhang, and W. Hanke, *Phys. Rev. B* **85**, 180502 (2012).
- [32] M. Khodas and A. V. Chubukov, *Phys. Rev. Lett.* **108**, 247003 (2012).

- [33] S.-L. Yu, J. Guo and J.-X. Li, J. Phys.: Condens. Matter **25**, 445702 (2013).
- [34] R. M. Fernandes and A. J. Millis, Phys. Rev. Lett. **110**, 117004 (2013).
- [35] F. F. Tafti, A. Juneau-Fecteau, M.-È. Delage, S. René de Cotret, J.-Ph. Reid, A. F. Wang, X.-G. Luo, X. H. Chen, N. Doiron-Leyraud, and L. Taillefer, Nat Phys **9**, 349 (2013).